Supplementary Information

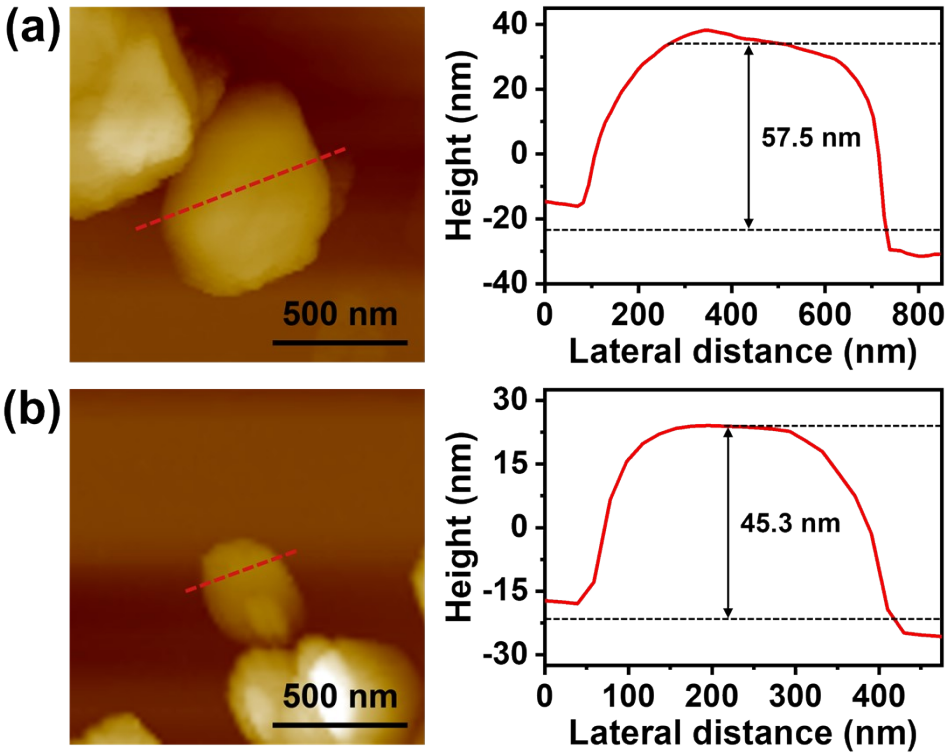

Fig. S1. AFM images and height profiles of 2D-assembled PG nanoparticles.

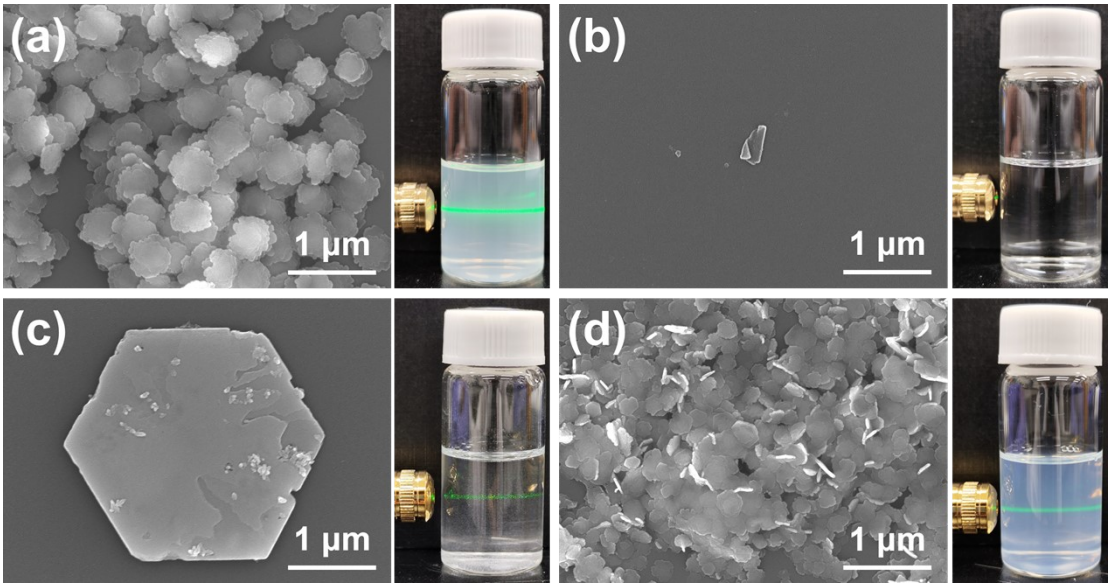

Fig. S2. SEM images of PG nanostructures and photographs of laser-exposed PG structure suspensions, synthesized under different solvent compositions at constant precursor content. The precursor : water : organic solvent volume ratio is (a) 1 : 1 : 11 (with water in ethanol), (b) 1 : 0 : 12 (without water in ethanol), (c) 1 : 12 : 0 (without ethanol in water), and (d) 1 : 1 : 11 (with water in acetone).

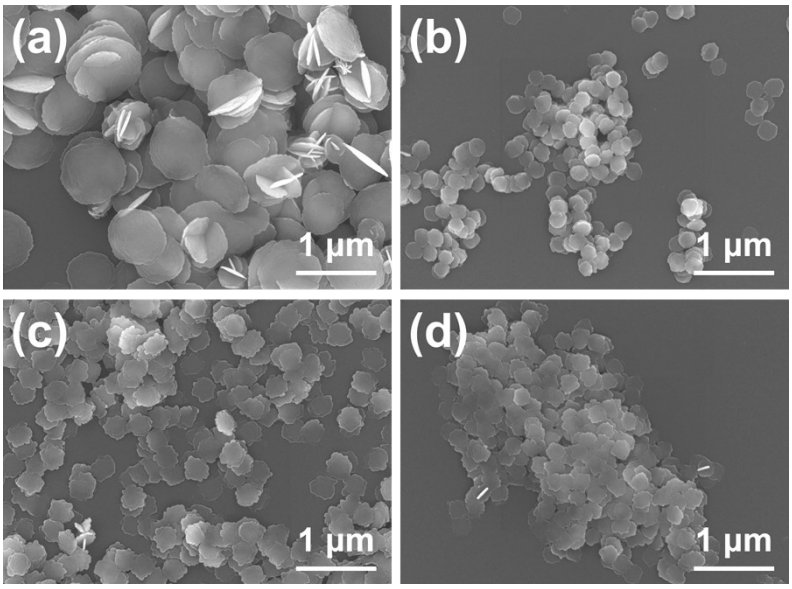

Fig. S3. SEM images of PG nanoparticles synthesized with constant precursor : water : alcohol volume ratio of 1 : 1 : 11 using different alcohol solvents: (a) methanol, (b) ethanol, (c) 1-propanol, and (d) 1-butanol.

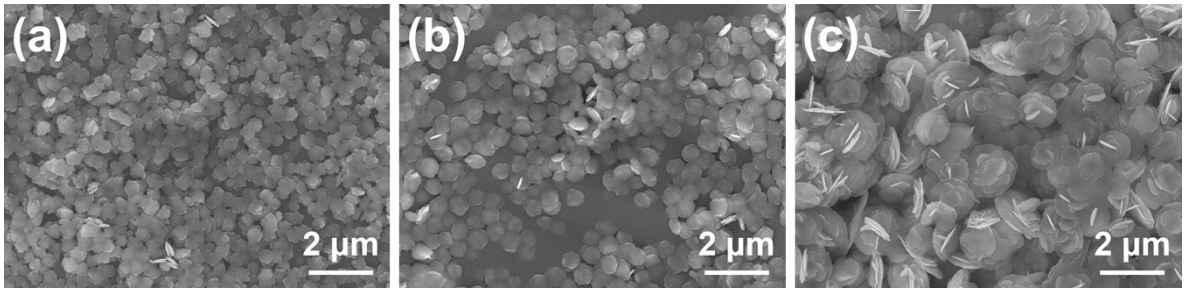

Fig. S4. SEM images of PG nanoparticles synthesized at constant precursor : water : alcohol volume ratio of 1 : 1 : 11 with increasing Pb concentration of precursor solution: (a) 0.015, (b) 0.074, and (c) 0.148 M

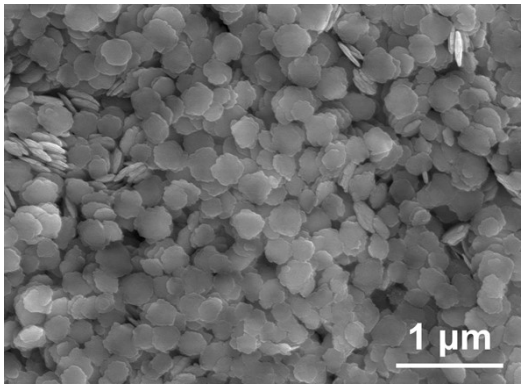

Fig. S5. SEM images of 2D-assembled PG nanoparticles using ammonia as a basic catalyst.

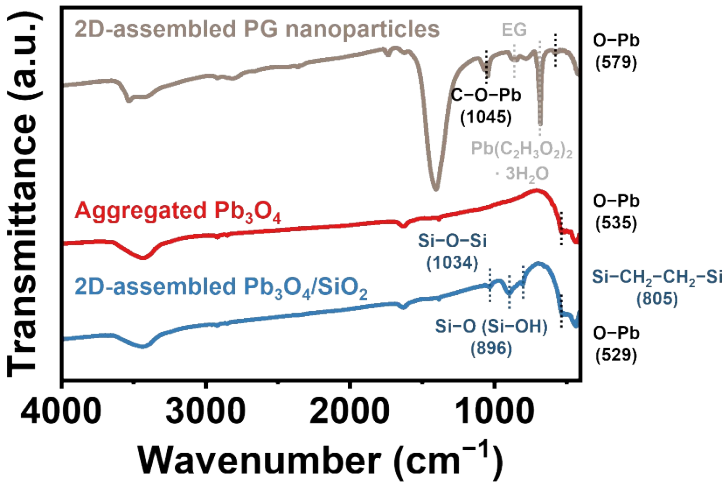

Fig. S6. FT-IR spectra of 2D-assembled PG nanoparticles, aggregated Pb_3O_4, and 2D-assembled Pb_3O_4/SiO_2.

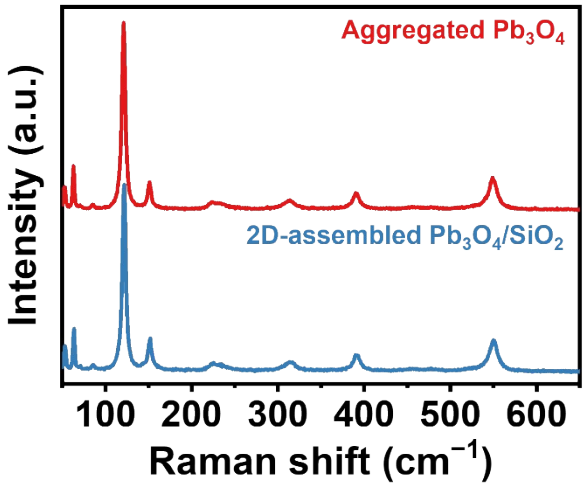

Fig. S7. Raman spectra of aggregated Pb_3O_4 and 2D-assembled Pb_3O_4/SiO_2.

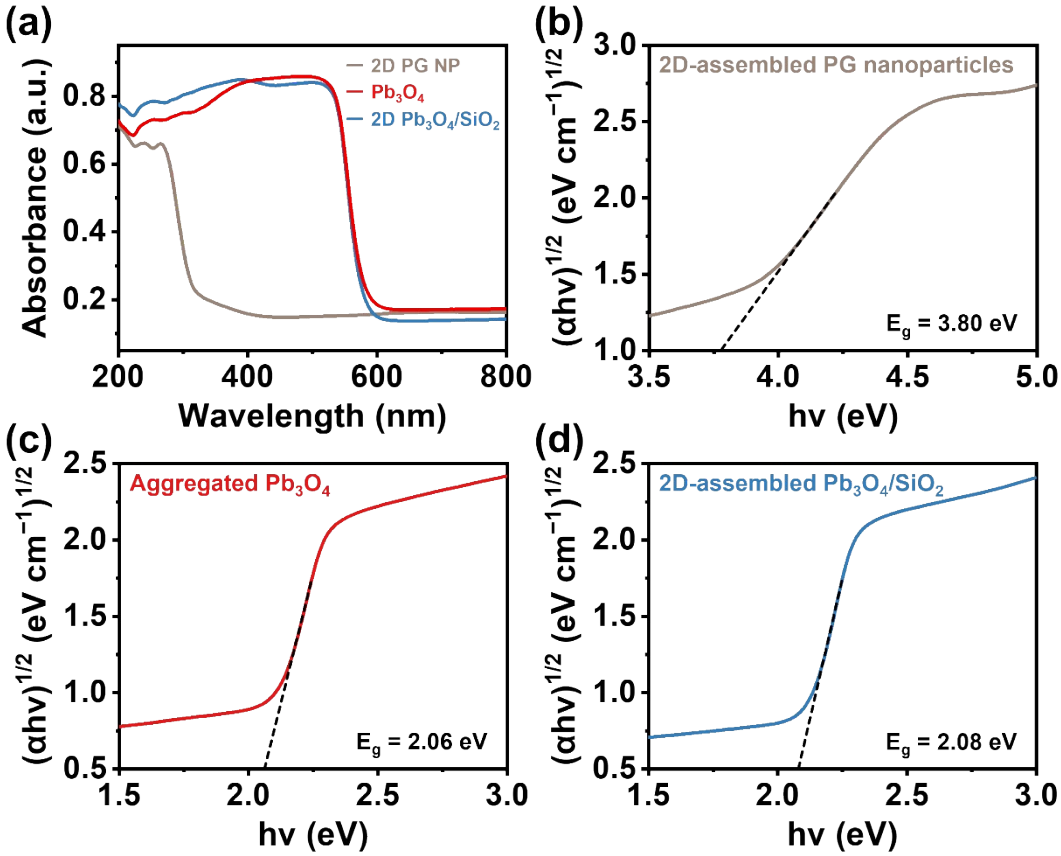

Fig. S8. (a) UV-Vis diffuse reflectance spectra and Tauc plots of (b) 2D-assembled PG nanoparticles, (c) aggregated Pb_3O_4, and (d) 2D-assembled Pb_3O_4/SiO_2 (E_g = bandgap).

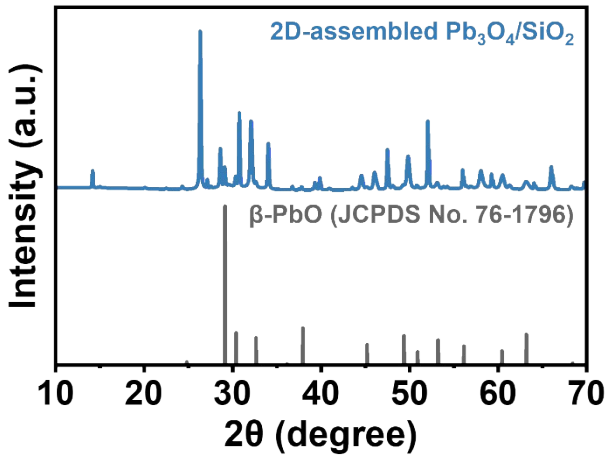

Fig. S9. XRD pattern of 2D-assembled Pb_3O_4/SiO_2 with weak β-PbO reflections.

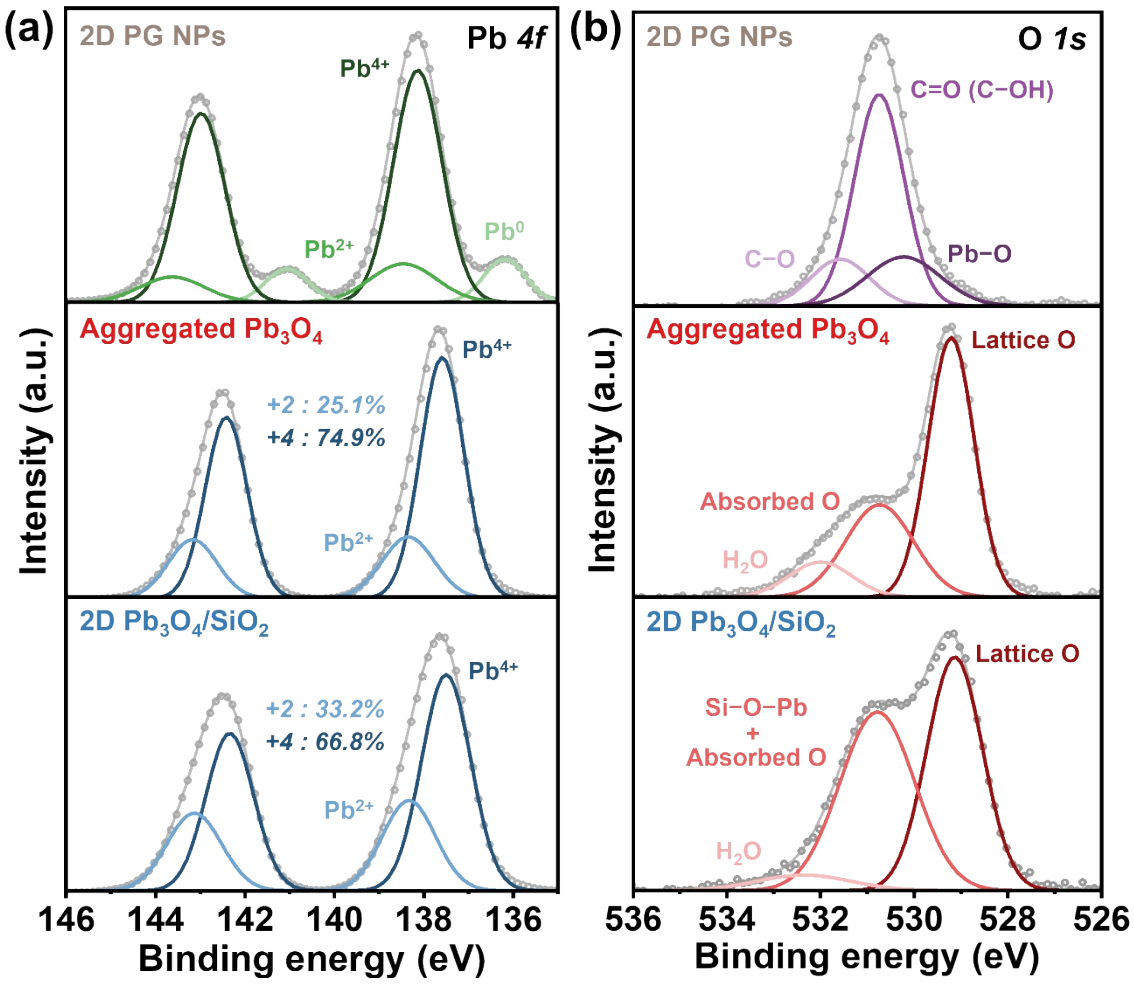

Fig. S10. (a) Pb 4f and (b) O 1s XPS spectra of 2D-assembled PG nanoparticles, aggregated Pb_3O_4, and 2D-assembled Pb_3O_4/SiO_2.

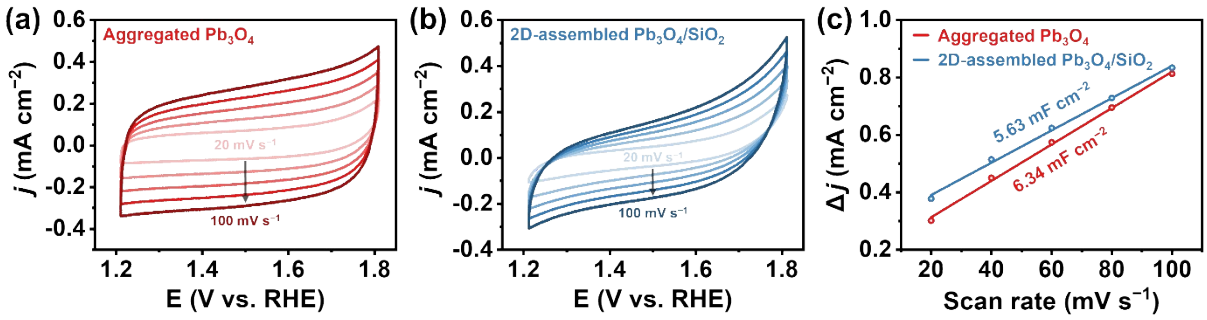

Fig. S11. (a,b) CV curves at different scan rates of 20, 40, 60, 80, 100 mV s^{-1} and (c) corresponding C_{dl} of aggregated Pb_3O_4 and 2D-assembled Pb_3O_4/SiO_2.

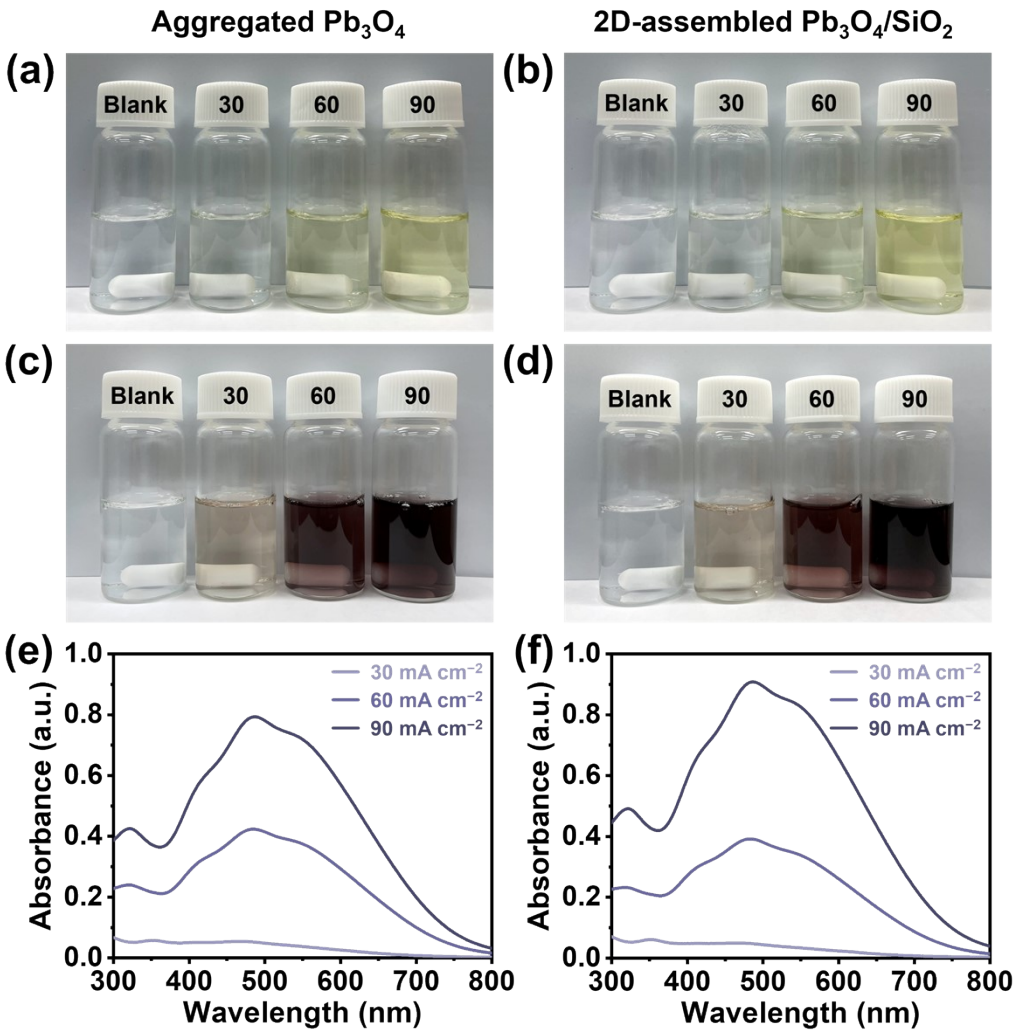

Fig. S12. Qualitative comparison of ozone formation at different current densities. Electrolyte color change after (a, b) KI addition and (c, d) KI and starch addition. UV–Vis absorption spectra of electrolytes obtained from (e) aggregated Pb_3O_4 and (f) 2D-assembled Pb_3O_4/SiO_2 anodes.

Table S1. Crystallite sizes calculated by the Scherrer equation for selected diffraction planes of aggregated Pb_3O_4 and 2D-assembled Pb_3O_4/SiO_2.

Diffraction plane	Crystallite size (nm)	
	Aggregated Pb_3O_4	2D Pb_3O_4/SiO_2
(110)	72	71
(211)	42	50
(202)	36	45

Table S2. Comparison of overpotential values for EOP with previously reported lead oxide-based catalysts.

Catalysts	Overpotential (V)	Reference
2D-assembled Pb_3O_4/SiO_2	**2.77**	**This work**
Pb_2O_3@Bi_2O_3−tube	3.26	[1]
β−PbO_2/Ta_2O_5 nanorods	2.90	[2]
$Bi_{12}PbO_{20}$	2.69~2.84	[3]
$Bi_6Pb_2O_x$	2.77	[4]
Commercial Pb_3O_4	2.73	[5]
β−PbO_2−120 nanorods	2.63	[6]
Cubic Pb_3O_4@SiO_2	2.61	[7]
Commercial β-PbO_2	2.51	[5]
PbO_2 nanorods	2.06	[8]

References

1 H. Shi, X. Wang, X. Peng, M. Xue, Y. Xue, F. Gao, X. Zhong, J. Wang, *J. Mater. Chem. A*, 2024, **12**, 10852-10862.

2 Y. Yan, Y. Gao, H. Zheng, B. Yuan, Q. Zhang, Y. Gu, G. Zhuang, Z. Wei, Z. Yao, X. Zhong, X. Li, J. Wang, *Appl. Catal. B*, 2020, **266**, 118632.

3 H. Shi, G. Feng, S. Li, J. Liu, X. Yang, Y. Li, Y. Lu, X. Zhong, S. Wang, W. Jianguo, *J. Mater. Chem. A*, 2022, **10**, 5430-5441.

4 H. Shi, G. Feng, T. Sun, X. Wang, L. Ding, Z. Wang, H. Jin, Q. Chen, S. Wang, X. Zhong, Y. Zhu, J. Wang, *Chem Catal.*, 2023, **3**, 100728.

5 J. Liu, S. Wang, Z. Yang, C. Dai, G. Feng, B. Wu, W. Li, L. Shu, K. Elouarzaki, X. Hu, X. Li, H. Wang, Z. Wang, X. Zhong, Z. J. Xu, J. Wang, *EES Catal.*, 2023, **1**, 301-311.

6 W. Jiang, S. Wang, J. Liu, H. Zheng, Y. Gu, W. Li, H. Shi, S. Li, X. Zhong, J. Wang, *J. Mater. Chem. A*, 2021, **9**, 9010-9017.

7 J. Liu, C. Qiu, Z. Xu, M. Xue, J. Cai, H. Shi, L. Ding, X. Li, X. Zhong, J. Wang, *Chem. Eng. J.*, 2023, **468**, 143504.

8 X. Wang, D. Wu, H. Ge, L. Wang, X. Wu, *J. Environ. Chem. Eng.*, 2023, **11**, 110248.